

# Refractive index sensor based on terahertz metamaterial absorber

A. ELAKKIYA, C. T. KALAIVANI\*

*Department of ECE, Saveetha Engineering College, Thandalam, Chennai, 602 105, India*

For refractive index sensing applications, a simple Terahertz (THz) Metamaterial Absorber (MMA) is proposed. Without using the multiple layers and multiple resonator processes, the numerical simulation results demonstrate that the absorber has six separate absorption peaks ranging from 0.74 THz to 0.95 THz. Electric and magnetic field distributions are used to examine the structure's physical mechanism. We describe the results of one THz MMA structure in this paper, focusing on two key device aspects: polarization ( $\phi$ ) and incident angle ( $\theta$ ) insensitivity, as well as sensing application at a fixed over-layer thickness, the proposed MMA resonant frequency is sensitive to the surrounding medium Refractive Index (RI). By adjusting the analyte RI value, the structure's performance parameters such as Q-factor, Figure of Merit (FOM), Sensitivity (S), and Full Width Half Maximum (FWHM) are explored using a numerical technique. Through a RI range of 1 to 1.41 at a fixed over-layer thickness of  $1\mu\text{m}$ , the reported MM design provided a RI sensor with a high sensitivity of 940 GHz/RIU, a Q-factor of 323, and a FOM of 393. The RI values are based on the RI values of biological samples. As a result, the MMA-based sensor reported here can be employed for biological applications as well as fluidic sample detection with extremely high sensitivity. We compared the six absorption peaks FOM, Q-factor, and S-values in this work with previously published publications, as well as the resonant frequency ranges, sensing results, and number of bands.

(Received October 6, 2022; accepted June 9, 2023)

*Keywords:* Ultra-sensitivity, Six-bands, Metamaterial absorber, Terahertz

## 1. Introduction

Many resonance devices, such as switches, filters, antennas, absorbers, filters, waveguides, and phase shifters, are required to control and operate the incident electromagnetic (EM) wave at subwavelength THz dimensions [1-3]. MMAs have developed a lot of attention because they have a lot of potential applications in optical electronics, such as photovoltaic batteries and solar panels, super lenses, better resolutions, thermal radiation and imaging, invisibility cloaking, biomedical imaging, materials detection, negative refraction, and other areas [4-6]. In the year 2008, Landy et al. suggested a perfect MMA [7]. Many researchers then provide single band, broadband, and multiband MMAs employing multiple layers and coplanar or multiple resonators mechanisms. Both strategies increase the simulation time, fabrication cost, and complexity of the structure. It's still difficult to make multiband MMAs without stacking and a coplanar mechanism. Because of the limitations of several layers in an absorber structure or different sized resonators in a single unit cell, early research on multiband MMAs mostly focused on double-band, tri-band, and quad-band operation [8-11]. Wang et al. demonstrated a hexa-band MMA based on the stacked layer structure of multiple order metallic patches [12]. Verma et al. used a basic planar MMA structure to investigate the eight bands design [13]. Hu et al. [14] demonstrated an ultra-multiband MMA structure based on a metal groove structures. Simple structured multiple band MMAs with sensing capabilities that do not use multiple layers and coplanar or multiple resonators mechanisms are rarely

planned. Furthermore, more than four bands are required for selective thermal reduction, thermal imaging, and filtering applications. We created and analysed the multiple bands MMA with sensing properties based on these desires.

When utilised as a thermal emitter and detector, MMA's smaller absorption bandwidth resulted in improved Q-factor and time coherence. Narrowband MMA-based sensors are currently confronting two disadvantages: reduced FOM and complex unit cell construction, both of which are present both overseas and at home [15]. Achieving a high FOM is critical because a higher RI sensor FOM signifies better molecular detection sensing (S) performance in the biological field [16]. To improve FOM, either reduce bandwidth or increase sensitivity value. Devices that are more aware of industrialised faults, on the other hand, will offer a higher sensitivity value rather than tiny line widths. As a result, lowering the bandwidth is more important than increasing the sensitivity. Designing a smaller bandwidth MMA seems to imply that we can acquire more FOM and quality factor detecting devices. At the same time, it is too perfect to be insensitive to the incident wave's polarisation ( $\phi$ ), as this would eliminate the need for polarisation apparatus. When one polarised wave is incident on the test sample, the test sample's sensitivity value to polarisation also reveals that the sample has a significant difference in detection effect depending on its orientation in relation to the user. Polarization-insensitive designs, on the other hand, will have 100% absorption in all directions. Combining all of these characteristics, the development of a numerous single band absorber and sensor with

polarisation insensitivity and a simple construction remains a valuable research topic [17].

We propose a multiple band absorber with narrower BW based on the above mentioned necessities, using a single planar resonator construction. The suggested MMA has absorption rates of 81 percent, 98 percent, 96.5 percent, 96 percent, 72 percent, and 90 percent at six distinct frequencies: 0.749 THz, 0.772 THz, 0.856 THz, 0.876 THz, 0.921 THz, and 0.941 THz. 0.27 THz/RIU, 0.94 THz/RIU, 0.24 THz/RIU, 0.64 THz/RIU, 0.61 THz/RIU, and 130 GHz/RIU are the sensitivity (S) of the six modes. The second absorption peak has a higher Q-factor, sensitivity, and FOM value of 323, 940 GHz/RIU,

and 393 GHz/RIU, respectively, than the first. Table 1 shows that the given design has a number of advantages, including high absorptivity, sensitivity, and performance over a wide incident angle range, which are all mentioned in the literature survey [20–31]. In the parametric research section, we looked at how several geometrical characteristics can affect the device's absorption rate and frequency. Furthermore, the structure is incidence angle and polarisation insensitive. This six-band ideal absorber with a shorter bandwidth offers a wide range of applications, including chemical, fluidic, photodetectors, biological, and other bio-sensing applications.

Table 1. Comparison of RI, Q, S and FOM of different structures proposed in previous works

Ref.	RI (n) range	S	Q	FOM	t (μm)	f <sub>r</sub> (THz)	A (%)	Polarization stability
[20]	1-1.39	300 GHz/RIU	22.05	2.94	1	2.249	99	Insensitive
[24]	1-1.04	3.05 THz/RIU	98.33	101.67	-	2.95	97.8	-
[25]	1-15	7.66 GHz/PU	-	1.50	1	1.67	94.16	-
[26]	1-1.1	1.96 THz/RIU	296.2	229.04	-	2.45	98	-
[27]	1-1.1	2.2 THz/RIU	59.8	34	-	2.99	99.6	sensitive
[28]	1-1.10	1.6 THz/RIU	29	14.55	-	3.19	99	-
[29]	1-1.4	14.11 μm/RIU	-	3.6	-	-	-	Insensitive
[30]	1-1.8	163 GHz/RIU	7.036	2.61	45	0.637	-	-
[31]	1.6	5.96 GHz/ μm	60.09	-	0-16	1.731	96.4	Insensitive
[21]	1.4-2	139.2 GHz/RIU	-	-	50	0.76	-	-
[22]	1-2	0.662 THz/RIU	-	-	10	2.67	-	-
This work	1-1.41	940 GHz/RIU	323	393	1	0.772	98	Insensitive

f<sub>r</sub>=Resonance frequency, A-Absorptivity, S-Sensitivity, Q- Quality factor, FOM-Figure of Merit, RI=Refractive index, t=Analyte thickness

## 2. Structure and design

The suggested THz MMA's unit cell design is depicted in Fig. 1, and it consists of three layers: a patterned square shaped planar resonator layer, a polyimide dielectric layer, and a continuous copper ground plane. By integrating different sized resonators in a single unit cell or stacking different multiple layers in a structure to achieve multi-band resonance, the designed absorber can realise six different absorption curves with a single planar electric square resonator, as opposed to previous reported absorbers by integrating different sized resonators in a single unit cell or stacking multiple layers in a structure to obtain multi-band resonance. The structure gave a double band if the square shaped resonator had a radius of 0.24 mm (Structure-I), while the structure gave a triple band if the square shaped resonator had a radius of 0.2 mm (Structure-II). Six bands are obtained when Structure-II is removed from Structure-I. Copper is utilised for the top and bottom metal layers. A 0.125 mm polyimide substrate with a permittivity ( $\epsilon_0$ ) of 3.5 and a dielectric loss tangent ( $\tan \delta$ ) of 0.0027 was used. The ground layer and dielectric layer are each 0.5 mm thick.

Copper has a frequency-insensitive conductivity of  $\sigma=5.8 \times 10^7$  S/m. The six curves not only have a lot of absorption, but they can also have a lot of sensing quality in the over layer (analyte). Using commercially available Computer Simulation Technology (CST) Microwave Studio software, the sensing value, structural efficiency, and absorption behaviour may be illustrated. The simulations used a unit cell in the z-plane with a fully matched open layer boundary condition and periodic boundary conditions in the y- and x-directions. The absorption rate is computed using the formula  $Ab(\omega) = 1 - Re(\omega) - Tr(\omega)$ . Where Ab denotes absorption, Tr denotes transmission,  $\omega$  denotes angular frequency, and Re denotes reflection. Tr( $\omega$ ) equals zero because the ground metal layer's thickness is greater than its skin depth. Therefore, the closer absorption Ab( $\omega$ ) moves to one. Furthermore, not only do the six peaks have a very high Q-factor and FOM value, but they may also provide foretold sensing characteristics that correspond to a modest shift in the dielectric environment refractive index.

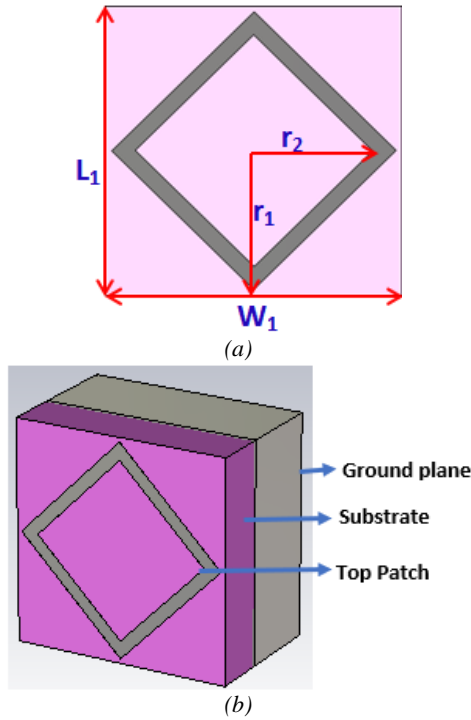


Fig. 1. (a) Proposed THz MMA-based RI sensor design; (b) 3D view of MMA (color online)

### 3. Results and discussions

#### 3.1. Absorption characteristics

The MMA is resonated at six different frequencies 0.749 THz, 0.772 THz, 0.856 THz, 0.876 THz, 0.921 THz and 0.941 THz with an absorption rate of 81 %, 98 %, 96.5 %, 96 %, 72 %, and 90 % respectively which is shown in Fig.2. These six frequencies are named as  $f_1$ ,  $f_2$ ,  $f_3$ ,  $f_4$ ,  $f_5$  and  $f_6$ . The FWHM value of these six modes is 0.00145,

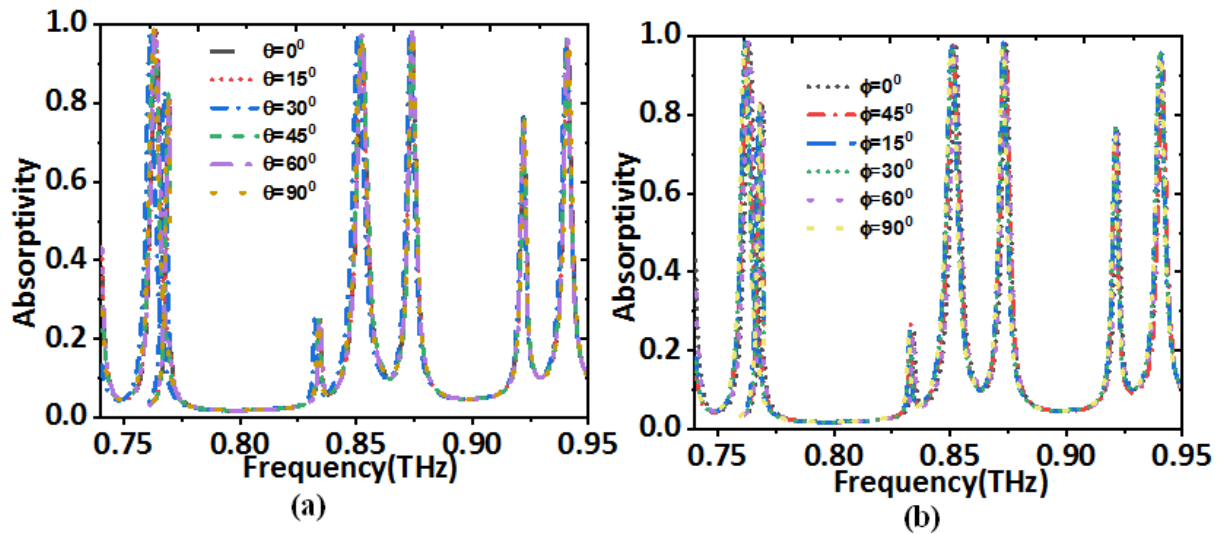


Fig. 3. Absorbance curves of the MMA for (a) different incident angle (b) different polarization angles under normal incidence condition (color online)

0.00239, 0.00247, 0.00287, 0.00474 and 0.00283. Because it provided the identical response in both transverse electric (TE) and transverse magnetic (TM) modes, the proposed structure is polarisation independent in nature (see Fig.2).

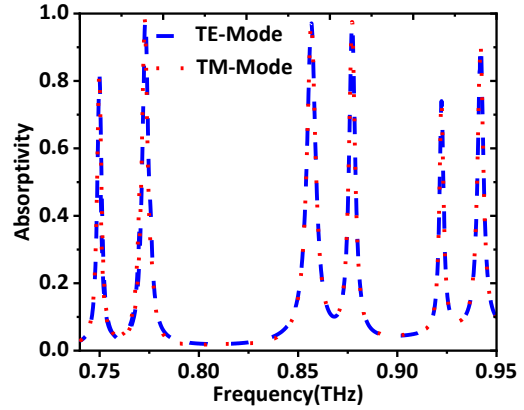


Fig. 2. Absorption spectra of the proposed MMA (color online)

#### 3.2. Polarization and angular stability

Fig. 3 (a) and (b) demonstrate the simulated absorbance characteristics of the proposed THz MMA, where the oblique incidence angle ( $\theta$ ) and polarization angle ( $\phi$ ) are changed from 0 to  $90^\circ$  in the frequency range of interest (0.75 to 0.95 THz). The structure's absorption and resonant frequency peaks did not change while the angle values were changed. As a result, the suggested MMA has outstanding polarization independent absorption characteristics. This is primarily due to the intended MMA's unit cell symmetry.

### 3.3. Electric field and magnetic field distribution

The main portion of the energy dissipation and absorption mechanism is the electromagnetic (EM) field. For six related frequencies, the method of E-field and H-field will be presented in this part.

The absorber, which was depicted in Fig.4, created the high E-field (a-f). The detention of electric field is done very well by the entire patch resonator and dielectric layer, as shown in Fig.4 (a), (c), (d), (e), and (f). And, as seen in Fig.4 (b), the E-field is greatest along the top and bottom edges of the patch structure, as well as at select points on the dielectric's surface.

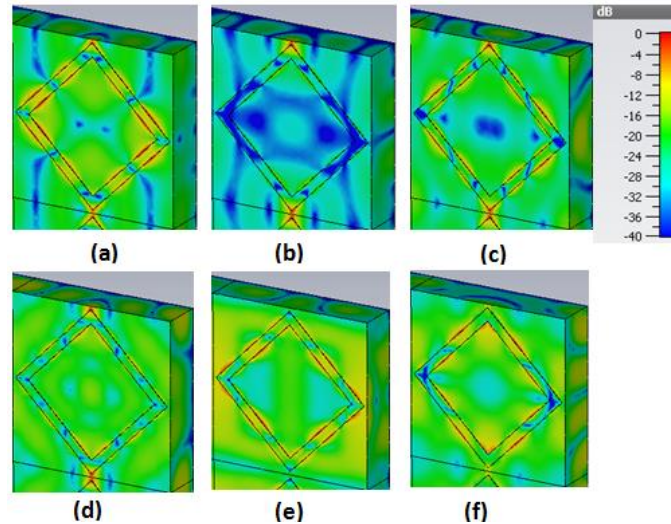


Fig. 4. Electric field distribution of six-band MMA (a) 0.749 THz, (b) 0.772 THz, (c) 0.856 THz, (d) 0.876 THz, (e) 0.921 THz, (f) 0.941 THz (color online)

The magnetic field distribution is utilised to examine the absorption method. The absorber, which was depicted in Fig.5, created the high H- field (a-f). The detention of magnetic field is done excellently by the entire patch

resonator and surface of the dielectric, as shown in Fig.5 (b), (d), (e), and (f). In addition, as shown in Fig. 5 (a) and (c), the H-field is greatest across the patch structure and at specific points on the dielectric's surface.

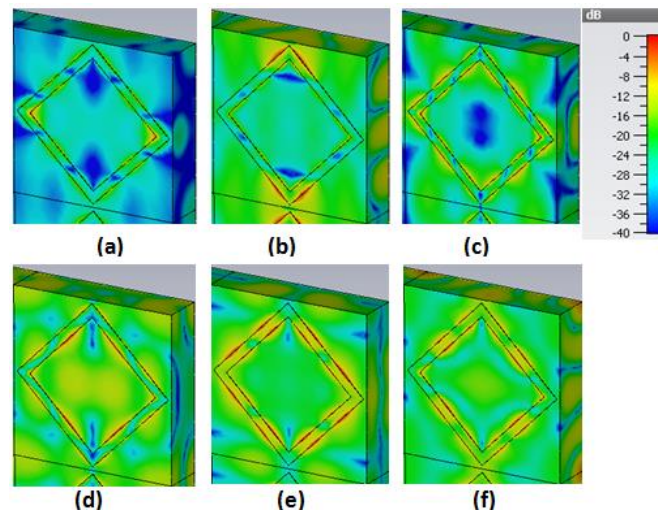


Fig. 5. Magnetic field distribution of six-band MMA (a) 0.749 THz, (b) 0.772 THz, (c) 0.856 THz, (d) 0.876 THz, (e) 0.921 THz, (f) 0.941 THz (color online)

### 4. Parametric study

Parameter studies can determine the best absorption value, resonance spots, and structural utilisation. Fig. 6

shows the result of the  $r_2$  on the absorption spectra when all other geometric factors are kept as constant.

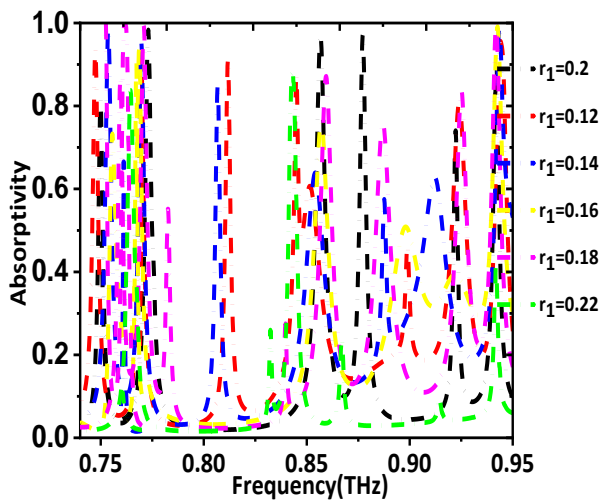


Fig. 6. Absorption curve as a function of radius  $r_2$  (color online)

Table 2. Number of resonant peaks with respect to radius  $r_2$

$r_2$ (mm)	No. of peaks	A (%)	RF (THz)
0.12	4	94, 79, 95, 92	0.811, 0.844, 0.923, 0.943
0.14	4	97, 85, 95, 99	0.753, 0.769, 0.806, 0.943
0.16	5	99, 75, 72, 94, 98	0.758, 0.767, 0.794, 0.856, 0.942
0.18	6	99, 76, 76, 86, 99, 84	0.758, 0.77, 0.858, 0.887, 0.925, 0.94
0.2	6	81, 98, 96.5, 96, 72, 90	0.749, 0.772, 0.856, 0.876, 0.921, 0.941
0.22	2	88, 84	0.773, 0.847
A-Absorptivity, RF-Resonant Frequencies			

## 5. Sensing mechanism

The quality factor is used to determine the MMA structure's sensing capabilities. Because the Q-value is a primary determining factor of the resonance point's benefit (and the definition of Q is the resonance frequency divided by its full width half maximum-FWHM). It may clearly state whether or not frequency can be used for sensing. When the Q-factor is larger, sensing performance improves [18]. The Q value is calculated for six frequency points: 516, 323, 346, 305, 194, and 332, as well as an explanation of the Q value. From low to high frequency, the six resonant frequencies are designated by the letters  $f_1$ ,  $f_2$ ,  $f_3$ ,  $f_4$ ,  $f_5$ , and  $f_6$ . Except for the fifth frequency mode, all of the frequency modes have a Q value greater than 300. In comparison to the other modes, the first mode has the highest Q-factor value. The design of the six-band MMA is promising in sensor-related industries as a result of its high Q-factor.

The MMA resonated in numerous bands at different frequencies with maximum absorptivity when the  $r_2$  value was varied from 0.12 mm to 0.22 mm with a step size of 0.2 mm, as shown in Table 2. The number of resonance points and absorption peaks of the proposed six-band MMA depends considerably on the geometric factors of the unit-cell structure.

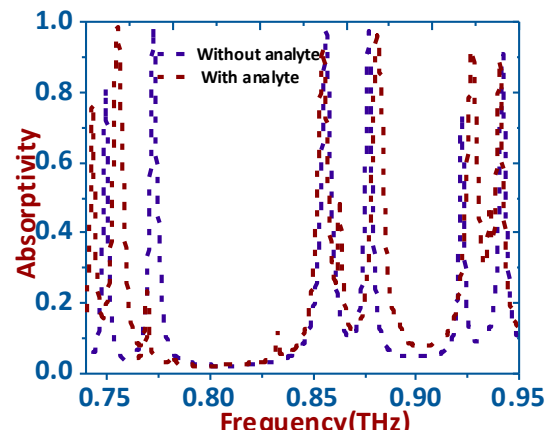


Fig. 7. Absorption spectra of the MMA coated without and with analyte layer (color online)

The sensing output of the suggested MMA was determined by analysing the absorption properties of the MMA. The top surface was coated with an unknown layer that was 1  $\mu\text{m}$  thick and varied in RI from 1 to 1.41 with a 0.01 step size. When the analyte is absent, the absorber shows six absorption peaks at 0.749 THz, 0.772 THz, 0.856 THz, 0.876 THz, 0.921 THz, and 0.941 THz. These six peaks are red displaced from their original position in Fig. 7 when 1  $\mu\text{m}$  analyte is placed over the top layer. Furthermore, the frequency redshifts of the six modes are 2.7 GHz, 9.4 GHz, 2.4 GHz, 6.4 GHz, 6.1 GHz, and 1.3 GHz, which are much higher than previously reported values. The increased dielectric constant generated by the presence of the analyte can be attributed to the obvious shift in this case [19]. As a result of the absorption peaks' shift characteristic, the suggested MMA may detect and sense the thickness ( $t$ ) and refractive index (RI) of thin films.

The sensing concept provided in this paper is based on changes in the environment's optical thickness, such as the RI ( $n$ ) and the thickness of the over layer ( $t$ ) implanted in the structure, which are intrinsic properties in biological or organic domains. The thickness of the analyte is 1  $\mu\text{m}$ , and the RI ranges from 1 to 1.41, which is comparable to several genuine biomaterials. T-type leukaemia infected person's blood has a refractive index of 1.39, while healthy person's blood has a refractive index of 1.35 in this study.

The normal basal cell concentration is 40-80 percent, with a refractive index of 1.36, while the impacted basal cell concentration is greater than 80 percent, with a refractive index of 1.38 [20]. In DNA, the refractive index can range from 1 to 1.4, while in RNA, it can range from 1.6 to 2 [21]. While adjusting the refractive index values, the resonant frequency value is red-shifted, as illustrated in Fig.8. Actually, the RI sensitivity ( $S$ ) is a sensitive factor in the resonance structure's illumination sensing technique, and the sensitivity may be described as  $S = df/dn$ , where  $dn$  is the RI change and  $df$  is the frequency change [22]. The six modes include sensitivity ratings of 0.27 THz, 0.94 THz, 0.24 THz, 0.64 THz, 0.61 THz, and 0.13 THz. The second frequency point  $f_2$  has ultra-high sensitivity of 940 GHz.

Aside from sensitivity, the FOM [23] is a more relevant component in determining sensor quality since it allows for a direct comparison of sensing amounts between different sensors.  $FOM = S/FWHM$  is the formula for calculating the FOM. Table 3 shows the FOMs of the frequency points ( $f_1$ - $f_6$ ) based on the  $S$  values and the FWHM of the six resonance modes. More crucially, the frequency point  $f_2$  has a much higher sensitivity, FOM, and Q-factor than prior efforts in the terahertz frequency range. The design of the six-band absorber is promising in sensor-related domains and applications as a result of these remarkable capabilities.

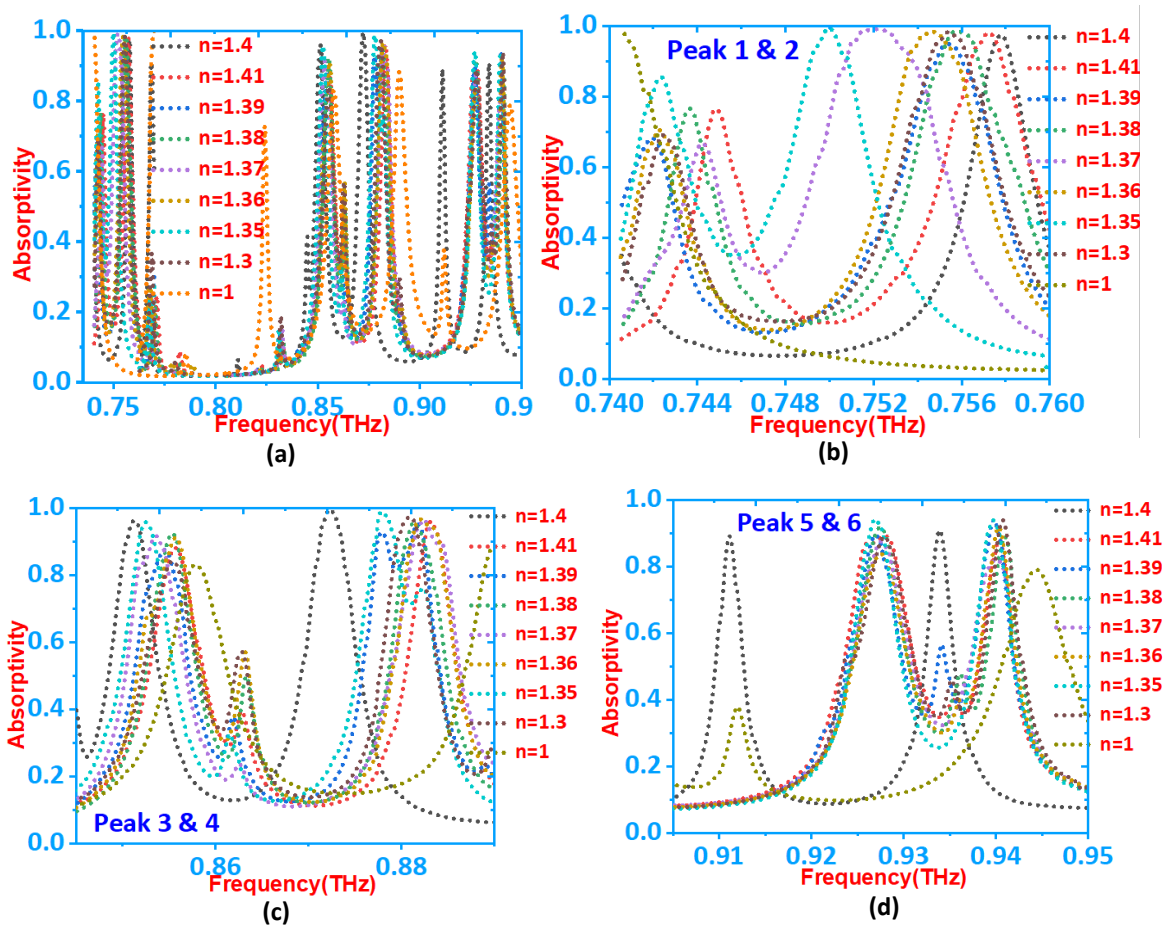


Fig. 8. (a) Absorption of the MMA sensor at different analyte refractive indices, (b) (c) (d) clear view of modes 1 & 2, 3 & 4, 5 & 6 respectively (color online)

Table 3. Q-factor, sensitivity and FOM values for six frequencies

$f_r$ (THz)	Resonant mode points	FWHM	$Q=f_r/\text{FWHM}$	$S=df/dn$ (THz/RIU)	FOM=S/FWHM
0.749	f1	0.00145	<b>516.9</b>	0.27	186.2
<b>0.772</b>	<b>f2</b>	<b>0.00239</b>	<b>323.3</b>	<b>0.94</b>	<b>393.3</b>
0.856	f3	0.00247	346.5	0.24	97.165
0.876	f4	0.00287	305.5	0.64	222.9
0.921	f5	0.00474	194.4	0.61	128.69
0.941	f6	0.00283	332.7	0.13	45.93

$f_r$ =Resonance frequency, A-Absorptivity, S-Sensitivity, Q- Quality factor, FOM-Figure of Merit, FWHM-Full Width Half Maximum

## 6. Conclusion

The biological applications of a Terahertz (THz) Metamaterial Absorber (MMA) based refractive index sensor are investigated. Using a single planar resonator, the numerical modelling results demonstrate that the absorber has six discrete absorption peaks ranging from 0.74 THz to 0.95 THz. At a fixed over layer thickness, the proposed MMA resonant frequency is sensitive to the surrounding medium Refractive Index (RI). The structure's performance metrics such as Q-factor, Figure of Merit (FOM), Sensitivity (S), and Full Width Half Maximum (FWHM) are examined using a numerical approach by modifying the analyte RI value. Through a RI range of 1 to 1.41 at a fixed over layer thickness of 1 $\mu$ m, the reported MM design provided a RI sensor with a high sensitivity of 940 GHz/RIU, a Q-factor of 323, and a FOM of 393. The RI values are based on the RI values of biological samples. As a result, the MMA-based sensor reported here can be employed for biological applications as well as fluidic matter detection with extremely high sensitivity. The six absorption peaks FOM, Q-factor, and S-values are compared with previously published papers, as are the resonant frequency ranges, sensing results, and number of bands. Electric and magnetic field distributions are used to investigate the structure's physical mechanism.

## References

- [1] H. Masanori, Jpn. J. Appl. Phys. **54**, 120101 (2015).
- [2] M. Tonouchi, 2007 19th International Conference on Applied Electromagnetics and Communications Dubrovnik, 1 (2007).
- [3] P. H. Siegel, IEEE Trans. Microw. Theory Tech. **52**, 2438 (2004).
- [4] P. H. Siegel, Terahertz technology. IEEE Trans. Microw. Theory Tech. **50**, 910 (2002).
- [5] D. M. Mittleman, J. Appl. Phys. **122**, 230901 (2017).
- [6] A. Redo-Sanchez, X.-C. Zhang, IEEE Journal of Selected Topics in Quantum Electronics **14**, 260 (2008).
- [7] N. I. Landy, S. Sajuyigbe, J. J. Mock, D. R. Smith, W. J. Padilla, Phys. Rev. Lett. **100**, 207402 (2008).
- [8] X. Shen, Y. Yang, Y. Zang, J. Gu, J. Han, W. Zhang, T. J. Cui, Appl. Phys. Lett. **101**, 154102 (2012).
- [9] Q. Y. Wen, W. Z. Hua, Y. S. Xie, Y. Q. Hu, L. Y. Li, Appl. Phys. Lett. **95**, 241111 (2009).
- [10] Y. Ma, Q. Chen, J. Grant, S. C. Saha, A. Khalid, D. R. S. Cumming, Opt. Lett. **36**, 45 (2011).
- [11] Y. Y. Lu, J. N. Li, S. H. Zhang, J. H. Sun, J. Q. Yao, Applied Optics **57**, 6269 (2018).
- [12] Wang Ben-Xin, Wang Gui-Zhen, Sang Tian, Wang Ling, Sci. Rep. **7**, 41373 (2017).
- [13] V. K. Verma, S. K. Mishra, K. K. Kaushal, V. Lekshmi, S. Sudhakar, S. K. Mishra, B. Appasani, N. Gupta, Plasmonics **15**, 75 (2020).
- [14] Dan Hu, Hongyan Wang, Jingfeng Zhang, Zhi Wang, Xiwei Zhang, Qiaofen Zhu, J. Phys. D Appl. Phys. **53**, 27 (2020).
- [15] Yuyin Li, Ye Liu, Zhengqi Liu, Qian Tang, Leilei Shi, Qiqi Chen, Guozhen Du, Biao Wu, Guiqiang Liu, Lei Li, Appl. Phys Express **12**, 072002 (2019).
- [16] J. Greffet, R. Carminati, K. Joulain, J. Mulet, S. Mainguy, Y. Chen, Nature **416**, 61 (2002).
- [17] Z. Liu, E. Gao, X. Zhang, H. Li, H. Xu, Z. Zhang, X. Luo, F. Zhou, Nanoscale Res. Lett. **15**, 1 (2020).
- [18] Pan Miao, Su Zhicong, Yu Zhenfang, Wu Pinghui, Jile Huge, Yi Zao, Chen Zeqiang, Results Phys. **19**, 103415 (2020).
- [19] Abbas Alipour, Ali Mir, Ali Farmani. Opt Laser Technol. **127**, 10620 (2020).
- [20] S. Saadeldin, M. F. O. Hameed, E. M. A. Elkaramany, S. S. A. Obayya, IEEE Sens J. **19**, 7993 (2019).
- [21] Yahiaoui Riad, Tan Siyu, Cong Longqing, Singh Ranjan, Yan Fengping, Zhang Weili, J. Appl. Phys. **118**, 083103 (2015).
- [22] Yao Yuan, Li Shaopeng, Zhu Lei, Wu Fengmin, He Xunjun, Jiang Jiuxing, Integr. Ferroelectr. **190**, 149 (2018).
- [23] L. Cong, S. Tan, R. Yahiaoui, F. Yan, W. Zhang, R. Singh, Appl. Phys. Lett. **106**, 031107 (2015).
- [24] Q. Xie, G. Dong, B. Wang, W. Q. Huang, Nanoscale Res. Lett. **13**, 137 (2018).
- [25] C. Sabah, B. Mulla, H. Altan, L. Ozyuzer, Pramana - J. Phys. **91**, 17 (2018).
- [26] Ben-Xin Wang, Yuanhao He, Pengcheng Lou, Wenhui Xing, Nanoscale Advances **2**, 763 (2020).
- [27] Wang Ben-Xin, Zhai Xiang, Wang Gui-Zhen, Huang Wei-Qing, Wang Ling-Ling, J. Appl. Phys. **117**, 014504 (2015).
- [28] Wang Ben-Xin, Wang Gui-Zhen, Sang Tian, J. Phys. D Appl. Phys. **49**, 165307 (2016).

- [29] Yunping Qi, Yu Zhang, Chuqin Liu, Ting Zhang, Baohe Zhang, Liyuan Wang, Xiangyu Deng, Yulong Bai, Xiangxian Wang, *Results in Physics* **16**, 103012 (2020).
- [30] M. D. Rotaru, J. K. Sykulski, *IEEE Transactions on*

*Magnetics* **47**(5), 1026 (2011)

- [31] S. Tan, F. Yan, W. Wang, H. Zhou, Y. Hou, *J. Opt.* **20**, 055101 (2018).

---

\*Corresponding author: [elakkiyakapil@gmail.com](mailto:elakkiyakapil@gmail.com)